recovery energy environment economy
2011 CSPG CSEG CWLS Convention

Sonic Scanner Logging at Site C0009 of IODP Expedition 319, NanTroSEIZE

Hisao Ito*
Center for Deep Earth Exploration (CDEX)
Japan Agency for Marine-Earth Science and Technology (JAMSTEC)
3173-25 Showa-machi, Kanazawa-ku, Yokohama
Kanagawa 236-0001 Japan
hisaoito@jamstec.go.jp

Summary

As a part of the NanTroSEIZE program, operations during Integrated Ocean Drilling Program (IODP) Expedition 319 included riser drilling, analyses of cuttings and core samples, downhole measurements and logging, and casing at Site C0009 in the Kumano forearc basin. As a part of logging/ downhole experiments, FMI-Sonic Scanner was conducted. Sonic Scanner data was analyzed to study S wave anisotropy. Dispersion analysis was applied to find that stress induced anisotropy is dominant for almost entire depth interval. We also found intrinsic anisotropy for a limited depth interval. Anisotropy direction is almost N~W, which is almost in agreement with stress direction estimated from borehole breakouts. However we found slight difference between S wave anisotropy direction and stress direction, which might be due to presence of fracture system.

Introduction

Integrated Ocean Drilling Program (IODP) Site C0009 is located in the Kumano forearc basin. The purpose of this site was to secure a location for a long-term monitoring system in the hanging wall directly above the plate boundary where it is hypothesized to be inter seismically locked, conduct downhole measurements and wireline logging, and collect core and cuttings within the forearc basin and underlying units (Saffer et al., 2010).

Field Measurements

Lithology

Based on a range of data available from cuttings, core and wireline logging, four lithologic units at Site C0009 were differentiated using geological, geophysical, and geochemical characteristics. Unit I is composed of silty mud with abundant sandrich beds ranging up to 40 m in thickness. Unit II is composed dominantly of silty clay, with silt and sand interbeds and minor interbeds of volcanic ash. Unit III is composed of abundant silty clay and poorly lithified silty claystone, with interbeds of silt and fine sand layers. Unit IV is composed dominantly of silty claystone, with common silt interbeds, few poorly consolidated sand layers, and rare interbeds of fine vitric tuff. The Unit III/IV boundary is marked by an ~1.8 Ma hiatus (3.8–5.6 Ma).

Logging

Five wireline logging tool strings were used in Exp. 319: **A.** Environmental Measurement Sonde (EMS) –High-Resolution Laterolog Array (HRLA) –Platform Express (PEX)–gamma ray (GR). HGNS = Highly Integrated Gamma Ray Neutron Sonde, PEF = photoelectric effect, HRMS = High-Resolution Mechanical Sonde. **B.** Formation MicroImager (FMI)-Hostile Natural Gamma Ray Spectrometry Cartridge (HNGC)-Sonic Scanner-EMSPower Positioning Device and Caliper Tool (PPC). **C.** Modular Formation Dynamics Tester (MDT)-GR. **D.** Junk basket. CCL = casing-collar log. and **E.** Walkaway and zero-offset vertical seismic profile (VSP).

The FMI and SonicScanner were used in the same tool string.

Sonic Scanner

On board velocity analysis was made (Fig. *). The distinct featutures of th eVp and Vs results are

1) Large Vp decrease in Unit IIIB
2) Sharp chane at UnitIII/IV boundary
3) In the UnitIV, the log data show rogouse condition of the borehole

Sonic Scanner anisotropy Analysis

The Alford Rotation technique (Alford, 1986) is employed to transform the X and Y dipole data into a Fast and Slow Shear dipole data set. Additional outputs generated by this process are the Fast Shear Azimuth (FSH), Cross Energy Anisotropy and the Time Anisotropy.

Once the Fast and Slow shear waveforms are generated, these are each processed to give the DTshear-Fast and DTshear-Slow. The Slowness Anisotropy is computed from the difference of these two measurements.

Three measurements of anisotropy are computed. These are energy anisotropy, slowness anisotropy and time anisotropy**.**

Slowness anisotropy is the difference between the fast and slow slowness calculated by STC on the rotated waveforms. It yields a quantitative measure of slowness anisotropy, and has the best vertical resolution at about 3 ft [~ 1 m]; the total length of the receiver array. It can be compared directly with seismic or core measurements of slowness anisotropy.

$$ANI_{DT} = (DT_{Slow} - DT_{Fast})/((DT_{Slow} + DT_{Fast})/2)*100$$

Where:

ANI_{DT} : Slowness-based anisotropy

DT_{Slow} : Slow shear slowness

DT_{Fast} : Fast shear slowness

Traveltime anisotropy is the arrival-time difference between the fast- and slow-shear waves at the receivers. It is obtained from a cross-correlation between fast and slow shear-wave arrivals at each receiver spacing. Time lags computed at each receiver are referenced to the largest offset receiver and averaged across the receiver array. This is divided by the average of the fast and slow arrival times to compute a percentage difference. The traveltime anisotropy indicator is robust and quantitative, and has the vertical resolution of the average transmitter-receiver spacing, 13 ft [~ 4 m]. Slowness and traveltime anisotropy indicators are identical in formations with homogeneous beds thicker than 13 ft.

$$ANI_{TT} = TT_{Diff}/TT_{Fast}*100$$

Where:

ANI_{TT} : Time-based anisotropy

DT_{Slow} : Slow shear slowness

DT_{Fast} : Fast shear slowness

TT_{Diff} : Arrival time difference between fast and slow shear waves

TT_{Fast} : Fast shear arrival time

Energy anisotropy is the energy in the cross component waveforms as a percentage of energy in all four components. In an isotropic formation, energy anisotropy reads zero. In an anisotropic formation, the reading depends on the degree of anisotropy. Two curves are computed from the waveforms: minimum and maximum cross-energy. The maximum cross energy is one of three independent indicators of anisotropy. Cross energy exists, if shear wave splitting has occurred. It is also important that the minimum cross energy be zero along the entire log, since this means the Alford model has been satisfied.

Frequency-Slowness Analysis (Dispersion plots)

The frequency-slowness analysis can be used to distinguish intrinsic anisotropy from stress-induced anisotropy. For best results, this analysis is done for circular borehole without breakouts or holes deformation. This method is based on the fact that the stress-induced dipole anisotropy exhibits a characteristic crossover in frequency-slowness domain of the fast and slow

Results

Three types of anisotropy are correlative very well. All rotation data are quite reasonable without ones at the depth have fatal borehole rugosity.

The interval around 2975 m and from 3025 – 3070 m below sea surface has quite low anisotropy and Fast Shear Azimuth estimation is meaningless. From around 2800-2875 m, relatively higher anisotropy is observed and the other intervals without rugose zone show normal anisotropy. There are some irregular anisotropy and fast shear azimuth around at 3100 m. To interpret anisotropy in rugose zone, depth selection with good borehole condition will be required.

Dispersion plot can be used for classification of root cause of anisotropy and FAST and SLOW rotated flexural shear slowness quality check (and also all other slowness quality check, slowness types like Leaky and/or dispersion, parameter optimization and DTmud). As the result of shear slowness data quality check, FAST and SLOW shear slowness are biased to be higher slowness due to wide process frequency range. However it was tried to be improved, too narrow frequency range with weak energy level where shear slowness have constant value made it to be difficult to fit the parameters to the raw data at each depth in overall zoning interval. Therefore wider frequency setting picked up dispersive higher energy signals. Following figures show typical dispersion plots from anisotropy zones mentioned in chapter 4.3 with caliper data. Horizontal lines in second track are 1 m scale per each.

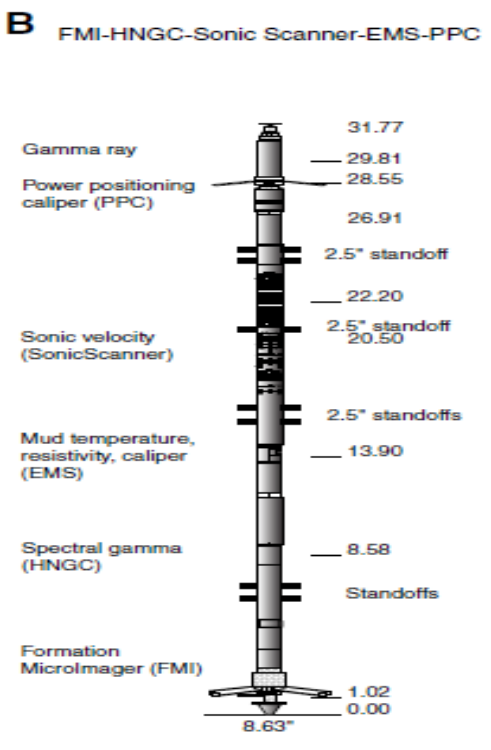

Figure 1: Five wireline logging tool strings were used in Exp. 319: The FMI and SonicScanner were used in the same tool string.

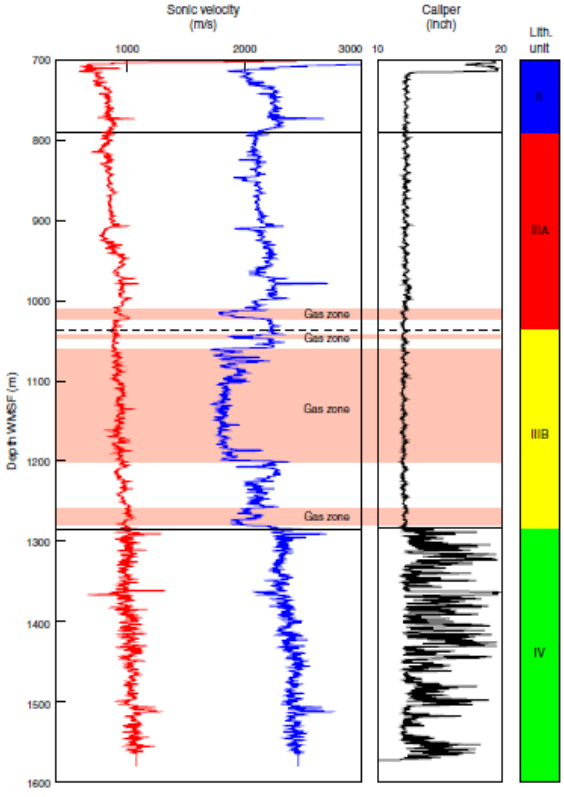

Figure 2: On board determination of Vp (blue) and Vs(red) by STC method. Note the extreme vigoursity of the borehole beeper than 1290 mbsf. II, IIIA, IIIb, IV show the geological and logging unit.

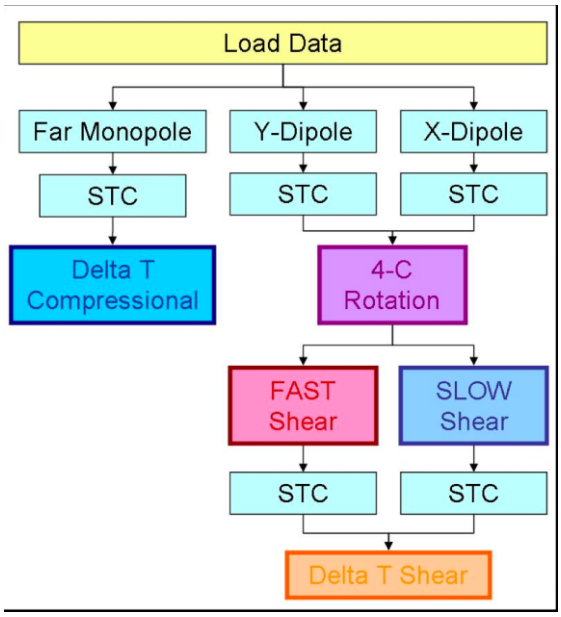

Figure 3: Sonic Scanner processing flowchart to obtain DT compressional and DT shear.

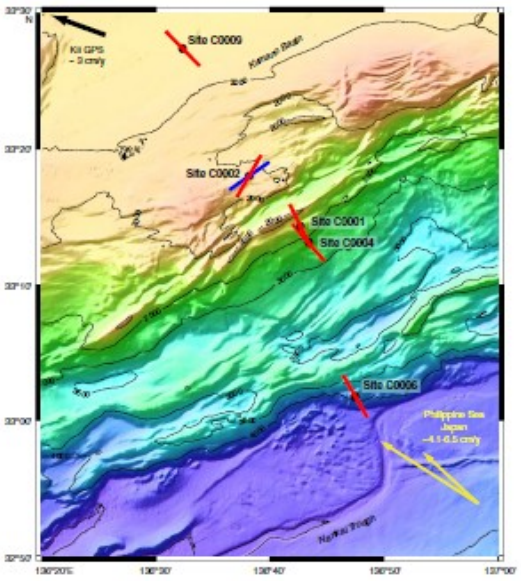

Figure 4: Orientation of Shmax determined from breakouts (Lin et al., 2010).

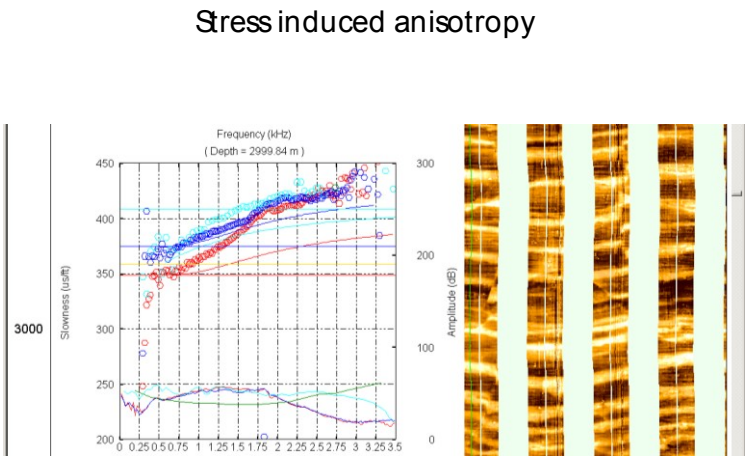

Figure 5: An example of dispersion analysis (left) and FMI (right).

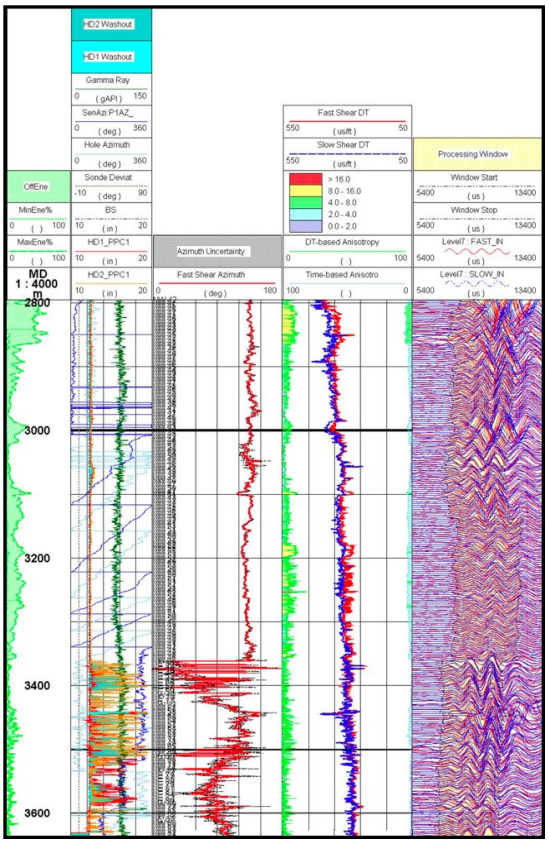

Figure 6: Anisotropy Post Process Plot. Third track shows FAST and SLOW shear slowness, Slowness based anisotropy and Time based anisotropy.

Conclusions

We find that stress induced anisotropy is dominant for almost entire depth interval. We also found intrinsic anisotropy for a limited depth interval. Anisotropy direction is almost N~W, which is almost in agreement with stress direction estimated from borehole breakouts for the depth shallower than 1280 mbsf (which corresponds to Unit IIIA and IIIB). For the depth interval deeper than 1280 mbsf, which corresponds to Unit IV:accretionary prism, the data quality was not enough to infer the anisotropy. However we might find slight S anisotropy azimuth rotation.The amount of stress anisotropy is 5~8 %.

Acknowledgements

We thank Moe Kyaw, Y. Sanada and Y. Kido for their excellent technical assistance in help.

References

Alford, R.M. “Shear Data in the Presence of Azimuthal Anisotropy: Dilley, Texas.” Expanded Abstracts, 56th SEG Annual International Meeting and Exposition, Houston, TX, Nov. 2-6, 1986, paper S9.6.

Lin, W., et al. (2010), Present day principal horizontal stress orientations in the Kumano forearc basin of the southwest Japan subduction zone determined from IODP NanTroSEIZE drilling Site C0009, Geophys. Res. Lett., 37, L13303, doi:10.1029/2010GL043158.

Saffer, D., McNeill, L., Byrne, T., Araki, Toczko, S., .Eguchi, N., Takahashi, K., and the Expedition 319 Scientists, Proceedings of the Integrated Ocean Drilling Program, Volume 319, 1-180, 2010.